Journal of Biomechanics 45 (2012) 997–1002

Contents lists available at SciVerse ScienceDirect

Journal of Biomechanics

journal homepage: www.elsevier.com/locate/jbiomech
www.JBiomech.com

Replicating a Colles fracture in an excised radius: Revisiting testing protocols

David W. Wagner*, Derek P. Lindsey, Gary S. Beaupre

VA Palo Alto Health Care System, Bone and Joint Center, 3801 Miranda Avenue, Building 51, Mail Stop 153, Palo Alto, CA 94304-1290, USA

ARTICLE INFO

Article history:
Accepted 7 January 2012

Keywords:
Distal radius
Colles fracture
Osteoporosis
Mechanical testing
Excised radius

ABSTRACT

A distal radius fracture in middle-age and older adults is often considered a sentinel indicator of osteoporosis. Mechanical testing of cadaveric specimens is often used to quantify bone strength and develop insight for relating in-vivo measures to fracture force. Mechanical testing protocols using an intact forearm have been successful at replicating a Colles fracture, however, excised isolated radius protocols based on the intact forearm testing protocol have not been as successful. One protocol originally designed to replicate the physiological condition of a fall on an outstretched hand was reproduced in our laboratory, yet surprisingly the produced distal radius fracture patterns were not consistent among specimens nor was dorsal angulation of the distal fragment that is characteristic of a Colles fracture observed. The purpose of this study was to perform a mechanics-based analysis of the excised radius loading protocol in order to quantify the imposed and internal forces on the radius. An idealized beam model of the excised radius revealed that in the area of the distal radius where Colles fractures occur, 99.99% of the maximum strain on the bone outer surface was the result of pure compressive loading. This loading condition is in direct contrast to the accepted mechanics of a Colles fracture, which is characterized as a metaphyseal bending fracture with the volar cortex failing due to tensile stresses and the dorsal cortex exhibiting compression and comminution. The results suggest that additional research, particularly related to overcoming the difficulties of reliably supporting and applying a force to the distal end of the radius, is necessary for clinical fracture patterns to be reliably reproduced with an excised radius mechanical testing protocol.

Published by Elsevier Ltd.

1. Introduction

In middle-age and older adults a distal radius fracture is often considered a sentinel indicator of osteoporosis. A common type of distal radius fracture is the Colles fracture. A Colles fracture occurs as a transverse fracture of the metaphyseal region of the distal radius, approximately 25–40 mm proximal to the radiocarpal joint, and can be identified with dorsal displacement and angulation of the distal fragment, radial shortening, and loss of radial inclination and palmar tilt (Colles, 1814; Goldfarb et al., 2001). Mechanistically, Colles fractures have traditionally been viewed as metaphyseal bending fractures with the volar cortex failing due to tensile stresses and the dorsal cortex exhibiting compression and comminution (Cooney et al., 1991; Crenshaw, 1998; Fernandez, 1993,2001; Jupiter and Fernandez, 1997). The typical cause of a Colles fracture is a fall on the outstretched hand with the wrist dorsiflexed.

Numerous investigators have used mechanical testing of cadaver specimens, typically the intact forearm or the excised radius, to assess various fracture-related properties of the distal radius. The objectives of these studies have included: quantifying bone strength (Eckstein et al., 2002; Lochmüller et al., 2002); correlating image-derived metrics to bone strength (Augat et al., 1998; Gordon et al., 1998; Louis et al., 1995; Muller et al., 2003; Myers et al., 1993,1991; Spadaro et al., 1994; Wu et al., 2000); and evaluating predictive models of bone failure (MacNeil and Boyd, 2008; Mueller et al., 2011; Pistoia et al., 2002; Varga et al., 2009,2011; Wigderowitz et al., 2000). Several laboratory methods have been specifically proposed for creating Colles-type fractures (Augat et al., 1998; Myers et al., 1991; Pistoia et al., 2002; Spadaro et al., 1994). Although some mechanical testing protocols that have used intact forearms have replicated Colles fracture patterns (Myers et al., 1991; Pistoia et al., 2002), protocols using the excised radius have not been as successful in consistently reproducing Colles fractures and the reasons for this are not well understood. Common protocols for preparing the excised radius for testing include potting of the proximal end of the radius (i.e., a fixed constraint), shallow potting of the distal end of the radius to provide an even distribution of the applied load, and a prescribed orientation (i.e., dorsal angulation and/or radial deviation) of the radius with respect to the applied load direction (Fig. 1). Muller et al. (2003) proposed a physiologically realistic excised radius

* Corresponding author. Tel.: 650 493 5000; fax: 650 849 0580.
E-mail address: dwwagner@va51.stanford.edu (D.W. Wagner).

0021-9290/$ - see front matter Published by Elsevier Ltd.
doi:10.1016/j.jbiomech.2012.01.014

protocol "to simulate a fall on an outstretched hand," with a displacement rate of 100 mm/sec. The bone orientation in their protocol was adapted from previous intact forearm cadaver studies (Augat et al., 1998; Myers et al., 1991) that positioned the arm with 15° of dorsal inclination from the vertical axis (and direction of the applied load).

Muller et al. (2003) stated that the "aluminum [potting] containers at each end of the radius prohibited reliable post-testing radiographs" and therefore the use of a conventional fracture grading system based on an observed fracture pattern was not possible. Instead, specimens with a fracture location outside the most-distal 10% of the radius were excluded (4 out of 38 specimens). The authors also noted that technical difficulties led to the exclusion of 13 additional specimens, resulting in a total of 17 specimens that were excluded. Slightly less than half of the original specimens were unavailable for analysis.

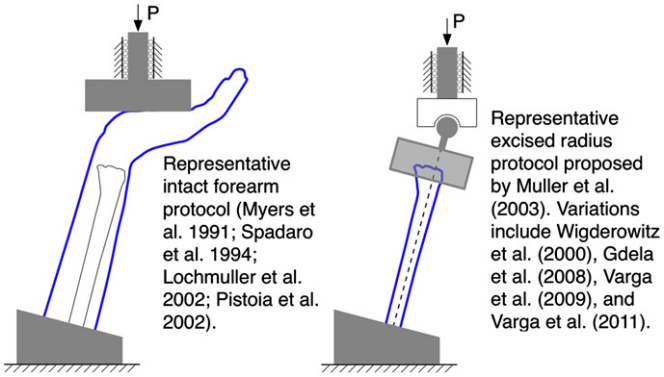

Fig. 1. Representative intact forearm and isolated, excised radius loading protocols for producing Colles-type fractures.

Table 1
Distal radius failure loads in axial compression and simulated fall conditions.

Study	Axial Compression (N)	Simulated Fall Condition (N)*
Eckstein et al. (2002)†	2630 ± 99	1595 ± 95
Lochmüller et al. (2002), (men)	3410	2230
Lochmüller et al. (2002), (women)	1870	1210

* The failure force for the simulated fall condition is the measured vertical load applied to the palmar surface of the hand (intact forearm) that resulted in a Colles fracture.

† Mean ± Standard Error.

Initial testing replicating the protocol described by Muller et al. (2003) in our laboratory resulted in fractures of the distal radius, however, the resulting fracture pattern was not consistent among specimens nor did we always observe the dorsal angulation of the distal fragment that is characteristic of a Colles fracture. Considering the range of failure forces that have been reported for several unique loading conditions of the radius (Table 1), it seems critical that mechanical testing protocols, particularly ones whose goal is to replicate a fracture pattern associated with a pathology, be well understood in how the applied forces are transferred to internal bone forces and subsequently result in a fracture. The purpose of this study is to perform a mechanics-based analysis of the loading protocol described by Muller et al. (2003) in order to identify the effects of the testing protocol on internal forces, compare with the mechanistic understanding of in-vivo failure previously described (Fernandez, 2001), and provide insight into features of a mechanical testing protocol that may be necessary for replicating a Colles-type fracture.

2. Methods

The isolated, excised radius loading protocol used by Muller et al. (2003) shares several common aspects from previous intact forearm loading protocols including a fixed constraint at the proximal end of the radius, a constrained applied vertical force, and the chosen angle of the forearm relative to the horizontal (Fig. 1). The position of the forearm posture is intended to replicate the impact posture during a fall on the outstretched hand and both the intact forearm and excised radius protocols have been implemented with the radius (or intact forearm) in 15 degrees of dorsal inclination from vertical. In the intact forearm protocol, loading occurs through a vertically applied force on the dorsiflexed palm while in the excised radius protocol, loading is applied through a shallowly potted portion of the distal radius that is allowed to freely rotate through a spherical joint between the loading platen and distal end of the radius (Fig. 1). Although the horizontal movement between the palmar surface and the loading platen in the intact forearm protocol is limited by pins extending from the loading platen into the soft tissue of palm, the compliance (and potential for movement) between the loading platen and the radius is greater than for the isolated, excised radius protocol, which has a direct connection between the loading platen and the radius through the spherical joint that prevents any transverse displacement. It is believed that the spherical cup that joins the distal end of the shallowly potted radius and the loading platen was originally intended to allow the distal end of the radius to freely rotate to replicate the kinematics of a Colles-type fracture (i.e. dorsal angulation of the distal fragment) in the same manner that the soft tissue of the palm and carpal bones allow for displacement of the distal fragment with respect to the radius and loading platen. Fig. 2 depicts an idealized structure that represents the excised radius loading protocol that will be solved using beam theory to provide insight into the internal and boundary forces imposed on the radius. In particular, the question of how the vertically applied

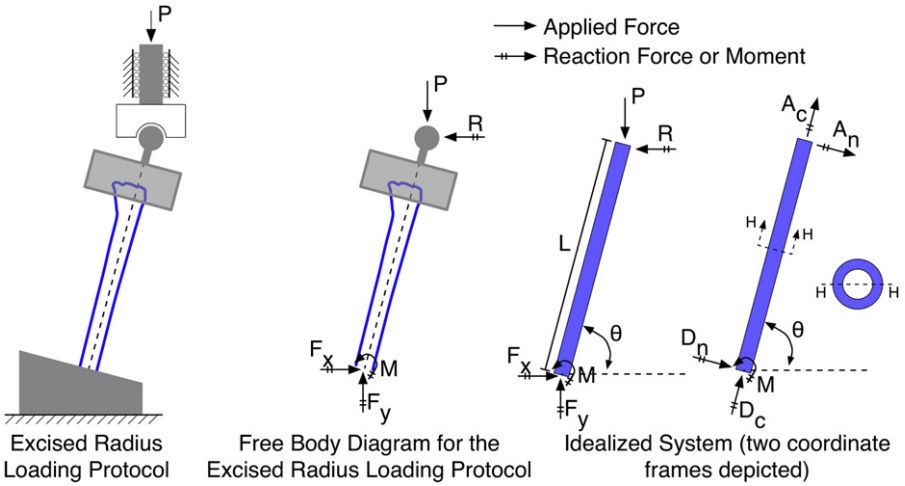

Fig. 2. Free body diagram of the isolated, excised radius loading protocol and a corresponding idealized beam structure with two coordinate frames.

force is distributed between compressive and bending loads (A_c and A_n, respectively in Fig. 2) is addressed.

The idealized structure of the radius is modeled as a homogenous beam with a hollow circular cross-section. The beam is oriented at 15° from the vertical axis and the proximal end is fixed while the distal end of the radius is free to rotate, but constrained to move along the vertical axis (Fig. 2). The beam structure is indeterminate in the first degree and the redundant reaction force is solved for using the force method (Popov and Balan, 1999). The general procedure of the force method as applied to the indeterminate system in Fig. 2 is listed in the Appendix. Two determinate structures (depicted as the primary and secondary structures in Fig. 3) are solved for independently and a structural compatibility equation, based on the allowed displacements of the original system, is implemented to resolve the redundant degree of freedom. To make the primary structure a determinate system, the redundant force R is removed. The secondary structure has the applied vertical force P removed and the reaction force R is applied as an external load.

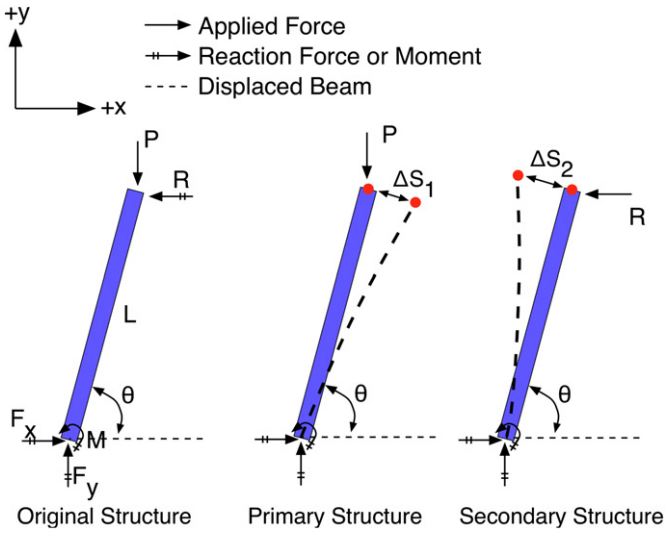

Fig. 3. Original indeterminate beam and the primary and secondary structures used with the force method used to solve for the indeterminate structure of the idealized system of the isolated, excised radius loading protocol.

The displacement of the primary (ΔS_1) and secondary (ΔS_2) structures is due to axial compression and bending components. The primary and secondary structure displacements due to axial compression (ΔC_1 and ΔC_2, respectively) and bending (ΔB_1 and ΔB_2, respectively) are solved for using beam theory. The resulting overall displacements of each structure (ΔS_1 and ΔS_2) are then solved using superposition. The structural compatibility equation (see Appendix for complete derivation), constrains the motion of the distal end of the beam in the x-direction:

$$\Delta S_{1x} + \Delta S_{2x} = 0. \quad (1)$$

The primary and secondary structure displacements in the x-direction (ΔS_{1x} and ΔS_{2x}, respectively) can be defined in terms of the derived displacements associated with the axial compression (ΔC_1, ΔC_2) and bending (ΔB_1, ΔB_2) components (Fig. 4).

Using those relationships, the following equations can be defined:

$$\Delta S_{1x} = -\Delta C_1 * \cos(\theta) + \Delta B_1 * \sin(\theta), \quad (2)$$

$$\Delta S_{2x} = -\Delta C_2 * \cos(\theta) - \Delta B_2 * \sin(\theta), \quad (3)$$

where, ΔC_1 is the displacement of the primary structure due to pure compression, ΔB_1 is the displacement of the primary structure due to bending, ΔC_2 is the displacement of the secondary structure due to pure compression, ΔB_2 is the displacement of the secondary structure due to bending, and θ is the orientation angle of the beam measured from horizontal.

Using equations (1)–(3), and the beam theory derived displacements (ΔC_1, ΔC_2, ΔB_1, ΔB_2, see Appendix for derivation), the reaction force R (Fig. 5) can be written as a function of the applied vertical load (P), orientation angle of the beam (θ), and several other beam properties (see Fig. 4 for a list). The vertically applied load P and the reaction force R are reformulated as axial compression (A_c) and normal (A_n) forces and depicted in Fig. 5.

3. Results

An idealized circular cross-section beam with a total length of 124 mm (L), inner radius of 2 mm, outer radius of 8 mm, and orientation angle of 75° (θ) was used to approximate the mechanical testing system previously described. The inner and outer radii were selected to approximate the cross-sectional area and

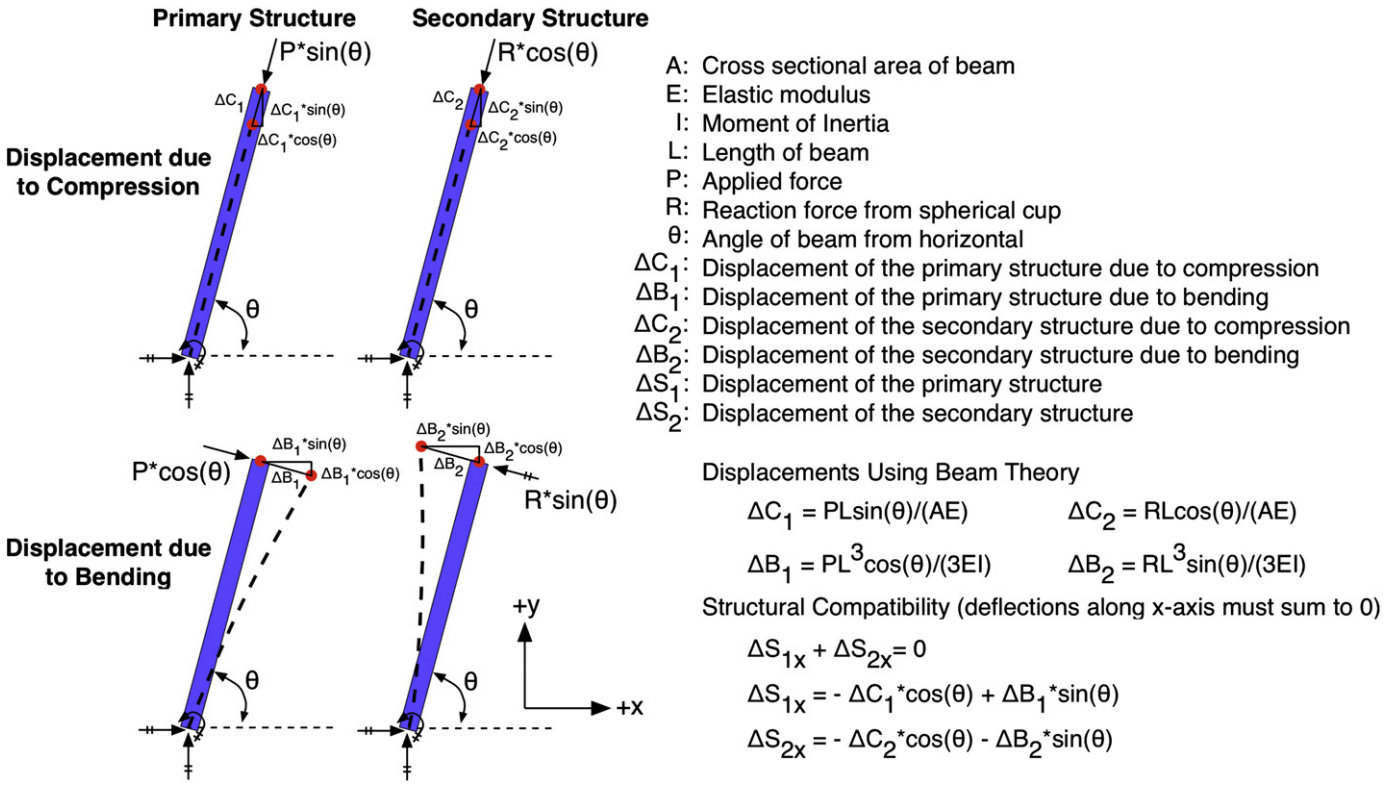

Fig. 4. Displacements and corresponding equations of the primary and secondary structures due to compression (axial) and bending (normal) loads.

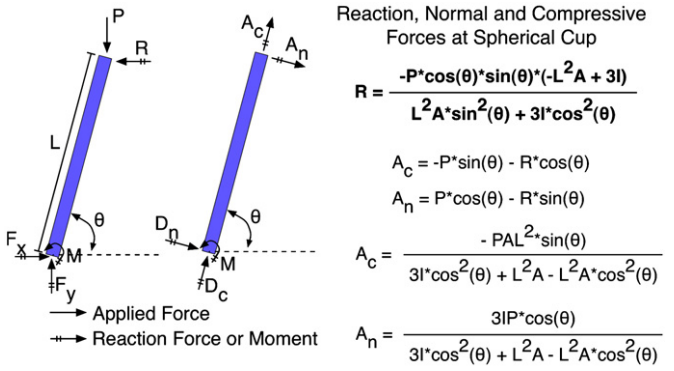

Fig. 5. Reformulation of the vertical and reaction forces to axial compression and normal forces of the idealized system representing the isolated, excised radius loading protocol.

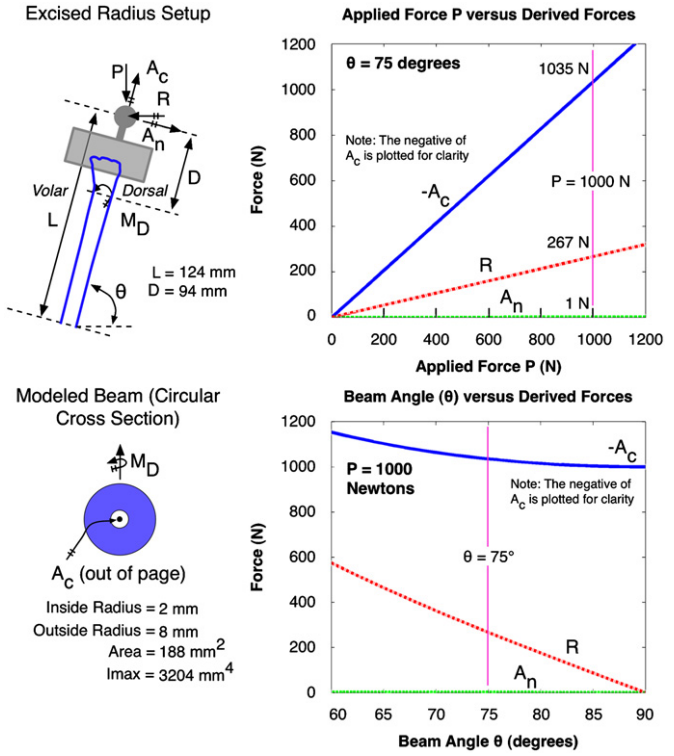

Fig. 6. Idealized beam model dimensions and model inputs. Plots of applied force (top right) and beam angle (bottom right) versus the axial compressive force (A_c), normal force (A_n), and reaction force (R) are depicted.

maximum moment of inertia of the distal radius (Augat et al., 1998). The total length L is approximated from the testing setup in our laboratory. The derived reaction (R), axial compression (A_c), and normal/bending (A_n) forces for the applied load (P) ranging from 0 to 1200 N are depicted in Fig. 6. The effect of orientation angle (θ ranging from 60° to 90°) on the same derived forces is also presented for a constant applied load (P) of 1000 N.

The normal strains for a circular cross-section located 94 mm (D) from the distal end of the idealized beam were calculated using the generalized flexure formula (Fig. 6). The distance D (94 mm) was selected to approximately correspond to the location a Colles-type fracture is traditionally observed. For the applied vertical force (P) of 1000 N, the compressive force (A_c) is -1035 N, the normal force (A_n) is 1 N, and the internal moment a distance D from the applied load is 86 N-mm. At the metaphyseal location corresponding to D, the compressive loading causes more than 99.99% of the maximum strain on the outer surface of the beam; less than 0.01% of the strain is caused by bending.

4. Discussion

A detailed analysis of a previously used excised radius protocol revealed that the internal forces imposed on the excised radius were primarily compressive. The axial compressive failure mode is contradictory to the reported bending failure mode attributed to Colles fractures (Fernandez, 1993). Although Eckstein et al. (2002) did report significant individual correlations between the failure loads corresponding to axial compression, 3-pt bending, and the simulated fall condition, with the highest correlation ($r^2=0.62$) occurring between the axial compression and 3-point bending conditions, the lack of transparency in replicating the correct failure mode (irrespective of whether a Colles fracture is replicated) should be addressed. As more advanced patient specific models are being developed to better predict fracture risk at the distal radius (Boutroy et al., 2007; MacNeil and Boyd, 2008; Mueller et al., 2011; Pistoia et al., 2002; Vilayphiou et al., 2011), there will be an increased need for precise validation. An excised radius mechanical testing protocol, in which soft tissues or the transmission of force through the carpal joint does not confound the forces applied to the radius, would be the natural choice for such a validation.

The limitation with excised radius protocols may be in part due to the difficulty in applying appropriate boundary conditions to replicate a bending moment at the distal end of the radius in the absence of soft tissue structures. For example, applying cantilever type bending (e.g., Fig. 4, primary structure) will produce an increasing internal moment along the radius shaft moving proximally. Such a loading protocol is likely to produce bending failures at the most proximal location where the bending moment in the largest. This may be one explanation for the excised radius protocol proposed by Varga et al. (2009) in which the authors state that the mechanical testing protocol was "designed to minimize bending at the proximal end [of the radius] and to have the maximum moment act on the epiphysis". When applying cantilever bending, bones that have a significantly lower metaphyseal bending strength (as compared to the diaphyseal bending strength) may still fracture in a Colles-type fracture.

The process of excising the radius and removing the connective soft tissue may also alter the supporting structure of the radius such that reliably replicating a Colles fracture pattern in the distal radius solely through artificial supports (i.e. shallowly potting the distal end of the radius) is not trivial. Although the intact forearm approach has shown efficacy in producing the Colles fracture pattern, the exact force directions and magnitudes imposed on the radius are often difficult to quantify (Augat et al., 1998). Changes in the off-axis forces have been shown to significantly effect predicted fracture strength (Troy and Grabiner, 2007). A combination of better defining the force imposed on the distal radius, limiting the confounding effects of soft tissue, and reducing the probability of other failure modes (prior to a Colles fracture) may have led to the development of the excised radius protocol proposed by Muller et al. (2003). In particular, the excised radius protocol allows for the application of high-speed displacements (100 mm/sec) to more accurately simulate a fall on the outstretched hand without the potential for confounding carpal bone fractures or dislocations.

One limitation with the evaluation presented here is that the idealized beam model of the excised radius assumed a prismatic beam with homogenous material properties. The actual application of the force method utilizes beam theory to calculate the

displacements of two derivative structures based on the original. The heterogeneous material and variable cross-section geometry of an actual radius would not precisely displace as does the idealized beam used in the calculations here. However, although the absolute magnitude of the compressive force to applied load may not be accurate, the relatively small ratio of normal load to compressive load at the distal end suggests that the overall failure mode is associated with axial compression and not bending.

Another limitation of the analysis presented here is that the dimensions of the structure analyzed were derived from a single laboratory experiment and potentially different configurations (i.e., by varying L, D, and θ) of the same setup may yield the appropriate mechanistic condition for replicating a Colles fracture. This is unlikely considering that the moment M_D depicted in Fig. 6 is positive and increases monotonically with the applied vertical force. Even if a change in configuration were able to elevate M_D to be the primary catalyst for failure, M_D is operating in the opposite direction for producing the dorsal displacement associated with a Colles-type fracture. A bending failure due to the positive moment M_D would result in a Smith-type fracture (i.e., volar displacement of the distal segment), which are not traditionally associated with a fall on the outstretched hand, but an impact to the back of the hand.

The boundary conditions of an excised radius loading protocol for producing fractures of the distal radius was evaluated in detail. Although upon casual inspection the boundary conditions seem similar to that of an intact forearm loading protocol known to replicate a Colles-type fracture, it has been shown that the failure mode imposed by that protocol is not consistent with the accepted mechanics of a Colles fracture. In particular, the spherical constraint at the distal end of the bone constrains the displacement of that end in the horizontal direction (perpendicular to the direction of the applied load) and essentially cancels out the bending moment supplied by the angled orientation of the bone resulting in a primarily compressive load being imposed on the radius. This loading condition is uniquely different than a fall on the outstretched hand of an intact radius, which does not have a similar artificial constraint (e.g., there is no inherent structure on the dorsal aspect of the intact radius that prevents the distal end of the radius from displacing dorsally when the arm is oriented at an angle and a compressive force is applied through the radial carpal joint). Subsequent excised radius loading protocols (Gdela et al., 2008; Pietruszczak and Gdela, 2010; Varga et al., 2009), although slightly different in configuration, have not completely addressed the unique aspect of applying the correct failure mechanism (i.e., bending versus axial compression) to the distal radius for reliably reproducing a Colles-type fracture. Additional research, particularly related to the support and boundary conditions of the distal end of the radius, is necessary for clinical fracture patterns to be reliably reproduced with an excised radius mechanical testing protocol.

Conflict of interest statement

The authors have no professional or financial conflicts of interest to disclose.

Acknowledgments

This study was supported by the Dept of Veterans Affairs, Rehab R&D Service (Proj. A6816R). We would like to thank Dr. Mary Bouxsein for discussing her experiences in replicating distal radius fractures with us.

Appendix A. Supplementary Information

Supplementary data associated with this article can be found in the online version at doi:10.1016/j.jbiomech.2012.01.014.

References

Augat, P., Iida, H., Jiang, Y., Diao, E., Genant, H.K., 1998. Distal radius fractures: mechanisms of injury and strength prediction by bone mineral assessment. Journal Of Orthopaedic Research 16, 629–635.

Boutroy, S., van Rietbergen, B., Sornay-Rendu, E., Munoz, F., Bouxsein, M.L., Delmas, P.D., 2007. Finite Element Analysis Based on In Vivo HR-pQCT Images of the Distal Radius Is Associated With Wrist Fracture in Postmenopausal Women. Journal Of Bone And Mineral Research 23, 392–399.

Colles, A., 1814. On the fracture of the carpal extremity of the radius. The Edinburgh Medical And Surgical Journal 10, 182–186.

Cooney III, W.P., Linscheid, R.L., Dobyns, J.H., 1991. Fractures and dislocations of the wrist. In: Rockwood, C.A., Green, D.P., Bucholz, R.W. (Eds.), Rockwood and Green's Fractures in Adults. JB Lippincott Company, Philadelphia, pp. 563–678.

Crenshaw, A.H., 1998. Fractures of shoulder girdle, arm, and forearm. In: Canale, S.T. (Ed.), Campbell's Operative Orthopaedics. Mosby, St. Louis, pp. 2281–2362.

Eckstein, F., Lochmüller, E.-M., Lill, C.A., Kuhn, V., Schneider, E., Delling, G., Müller, R., 2002. Bone strength at clinically relevant sites displays substantial heterogeneity and is best predicted from site-specific bone densitometry. Journal Of Bone And Mineral Research 17, 162–171.

Fernandez, D.L., 1993. Fractures of the distal radius: operative treatment. Instructional Course Lectures 42, 73–88.

Fernandez, D.L., 2001. Distal radius fracture: the rationale of a classification. Chirurgie De La Main 20, 411–425.

Gdela, K., Pietruszczak, S., Lade, P.V., Tsopelas, P., 2008. On Colles' Fracture: An Experimental Study Involving Structural and Material Testing. Journal Of Applied Mechanics 75. 031002-1-10.

Goldfarb, C.A., Yin, Y., Gilula, L.A., Fisher, A.J., Boyer, M.I., 2001. Wrist fractures: what the clinician wants to know. Radiology 219, 11–28.

Gordon, C.L., Webber, C.E., Nicholson, P.S., 1998. Relation between image-based assessment of distal radius trabecular structure and compressive strength. Canadian Association Of Radiologists Journal 49, 390–397.

Jupiter, J.B., Fernandez, D.L., 1997. Comparative classification for fractures of the distal end of the radius. The Journal Of Hand Surgery 22, 563–571.

Lochmüller, E.-M., Lill, C.A., Kuhn, V., Schneider, E., Eckstein, F., 2002. Radius bone strength in bending, compression, and falling and its correlation with clinical densitometry at multiple sites. Journal Of Bone And Mineral Research 17, 1629–1638.

Louis, O., Boulpaep, F., Willnecker, J., Van den Winkel, P., Osteaux, M., 1995. Cortical mineral content of the radius assessed by peripheral QCT predicts compressive strength on biomechanical testing. Bone 16, 375–379.

MacNeil, J.A., Boyd, S.K., 2008. Bone strength at the distal radius can be estimated from high-resolution peripheral quantitative computed tomography and the finite element method. Bone 42, 1203–1213.

Mueller, T.L., Christen, D., Sandercott, S., Boyd, S.K., van Rietbergen, B., Eckstein, F., Lochmüller, E.-M., Müller, R., van Lenthe, G.H., 2011. Computational finite element bone mechanics accurately predicts mechanical competence in the human radius of an elderly population. Bone 48, 1232–1238.

Muller, M.E., Webber, C.E., Bouxsein, M.L., 2003. Predicting the failure load of the distal radius. Osteoporosis International 14, 345–352.

Myers, E.R., Hecker, A.T., Rooks, D.S., Hipp, J.A., Hayes, W.C., 1993. Geometric variables from DXA of the radius predict forearm fracture load in vitro. Calcified Tissue International 52, 199–204.

Myers, E.R., Sebeny, E.A., Hecker, A.T., Corcoran, T.A., Hipp, J.A., Greenspan, S.L., Hayes, W.C., 1991. Correlations between photon absorption properties and failure load of the distal radius in vitro. Calcified Tissue International 49, 292–297.

Pietruszczak, S., Gdela, K., 2010. Inelastic Analysis of Fracture Propagation in Distal Radius. Journal Of Applied Mechanics 77. 011009-1-10.

Pistoia, W., van Rietbergen, B., Lochmüller, E.-M., Lill, C.A., Eckstein, F., Ruegsegger, P., 2002. Estimation of distal radius failure load with micro-finite element analysis models based on three-dimensional peripheral quantitative computed tomography images. Bone 30, 842–848.

Popov, E.P., Balan, T.A., 1999. Engineering Mechanics Of Solids, 2nd ed. Prentice-Hall, Upper Saddle River, New Jersey.

Spadaro, J.A., Werner, F.W., Brenner, R.A., Fortino, M.D., Fay, L.A., Edwards, W.T., 1994. Cortical and trabecular bone contribute strength to the osteopenic distal radius. Journal Of Orthopaedic Research 12, 211–218.

Troy, K.L., Grabiner, M.D., 2007. Off-axis loads cause failure of the distal radius at lower magnitudes than axial loads: a finite element analysis. Journal Of Biomechanics 40, 1670–1675.

Varga, P., Baumbach, S., Pahr, D., Zysset, P.K., 2009. Validation of an anatomy specific finite element model of Colles' fracture. Journal Of Biomechanics 42, 1726–1731.

Varga, P., Dall'ara, E., Pahr, D.H., Pretterklieber, M., Zysset, P.K., 2011. Validation of an HR-pQCT-based homogenized finite element approach using mechanical testing of ultra-distal radius sections. Biomechanics And Modeling In Mechanobiology 10, 431–444.

Vilayphiou, N., Boutroy, S., Szulc, P., van Rietbergen, B., Munoz, F., Delmas, P.D., Chapurlat, R., 2011. Finite element analysis performed on radius and tibia HR-pQCT images and fragility fractures at all sites in men. Journal Of Bone And Mineral Research 26, 965–973.

Wigderowitz, C.A., Paterson, C.R., Dashti, H., McGurty, D., Rowley, D.I., 2000. Prediction of bone strength from cancellous structure of the distal radius: can we improve on DXA? Osteoporosis International 11, 840–846.

Wu, C., Hans, D., He, Y., Fan, B., Njeh, C.F., Augat, P., Richards, J., Genant, H.K., 2000. Prediction of bone strength of distal forearm using radius bone mineral density and phalangeal speed of sound. Bone 26, 529–533.